Supramolecular self-assembly of EGCG-selenomethionine nanodrug for treating osteoarthritis

Haichao Yu [a,b,1], Zelong Song [a,b,1], Jie Yu [f,1], Boyuan Ren [g], Yuan Dong [b], Yonggang You [b], Zhen Zhang [b], Chengqi Jia [h], Yunpeng Zhao [e,*], Xuhui Zhou [d,**], Haifeng Sun [c,***], Xuesong Zhang [b,a,****]

[a] School of Medicine, Nankai University, Tianjin 300071, China
[b] Department of Orthopaedics, The Fourth Medical Center of PLA General Hospital, Beijing 100048, China
[c] School of Radiology, Shandong First Medical University and Shandong Academy of Medical Sciences, Shandong, 271016, China
[d] Department of Orthopaedics, Changzheng Hospital, Second Military Medical University (Naval Medical University), Shanghai, 200003, China
[e] Department of Orthopaedics, Qilu Hospital, Cheeloo College of Medicine, Shandong University, Shandong, 250012, China
[f] Peking Union Medical College Hospital, Chinese Academy of Medical Sciences and Peking Union Medical College, Beijing 100730, China
[g] Beijing Institute of Radiation Medicine, Beijing 100850, China
[h] Department of Orthopedics, Beijing Jishuitan Hospital, Beijing 100035, China

ARTICLE INFO

ABSTRACT

Osteoarthritis (OA) has emerged as a significant health concern among the elderly population, with increasing attention paid to ferroptosis-induced OA in recent years. However, the prolonged use of nonsteroidal anti-inflammatory drugs or corticosteroids can lead to a series of side effects and limited therapeutic efficacy. This study aimed to employ the Mannich condensation reaction between epigallocatechin-3-gallate (EGCG) and selenomethionine (SeMet) to efficiently synthesize polyphenol-based nanodrugs in aqueous media for treating OA. Molecular biology experiments demonstrated that EGCG-based nanodrugs (ES NDs) could effectively reduce glutathione peroxidase 4 (GPX4) inactivation, abnormal Fe^{2+} accumulation, and lipid peroxidation induced by oxidative stress, which ameliorated the metabolic disorder of chondrocytes and other multiple pathological processes triggered by ferroptosis. Moreover, imaging and histopathological analysis of the destabilization of the medial meniscus model in mice confirmed that ES NDs exhibiting significant therapeutic effects in relieving OA. The intra-articular delivery of ES NDs represents a promising approach for treating OA and other joint inflammatory diseases.

1. Introduction

Osteoarthritis (OA) is a prevalent chronic degenerative disease, significantly affecting more than 22% of individuals aged 40 years and more worldwide [1,2], thereby imposing a substantial economic burden on families and society [3]. OA is usually treated through conservative management with oral nonsteroidal anti-inflammatory drugs (NSAIDs) and assisted targeted exercise regimens, which effectively reduce pain and control OA progression [4,5]. However, prolonged use of NSAIDs can result in significant toxicities, such as gastrointestinal irritation and ulceration, bleeding, and azotemia, with decreased renal blood flow [4, 6]. Patients contraindicated for NSAIDs or who do not respond to them

may be considered for intra-articular corticosteroid injections as an alternative. Nevertheless, corticosteroids have the potential to accelerate cartilage degeneration [7]. Therefore, formulating safe and effective local treatment strategies according to the pathogenesis of OA not only mitigates patient complications but also optimizes therapeutic outcomes.

Age, obesity, and trauma are the primary causes of OA; however, recent studies have highlighted the close relationship between ferroptosis and the occurrence and progression of OA [8–10]. Ferroptosis is an iron-dependent new type of programmed cell death, which is different from apoptosis, necrosis, and autophagy [11]. The primary mechanism of ferroptosis involves the catalysis of lipid peroxidation in the cell membrane through the Fenton reaction mediated by divalent iron, ultimately leading to cell death [12]. Additionally, ferroptosis is characterized by a reduction in the levels of glutathione peroxidase 4 (GPX4), the core enzyme regulating the antioxidant system (glutathione system) [13,14]. The ferroptosis-induced metabolic imbalance of articular cartilage exacerbates the degradation of the extracellular matrix, resulting in decreased expression of key components, such as aggrecan (ACAN) and collagen-II (Col-2), and accelerating the progression of OA [10]. Consequently, reducing lipid peroxidation levels caused by iron-induced cell death in chondrocytes and enhancing GPX4 expression have emerged as critical therapeutic strategies for alleviating ferroptosis-induced OA.

Epigallocatechin-3-gallate (EGCG) is a natural antioxidant found in tea. It exhibits various biological activities such as antioxidant, anti-aging, and anti-inflammatory effects [15–17]. Furthermore, it protects the biological functions of adipose-derived mesenchymal stem cells (ADSCs) by clearing reactive oxygen species (ROS), which promotes cell proliferation, facilitates cartilage differentiation of ADSCs, and enhances

their capacity for joint cartilage repair [18]. A previous study demonstrated that EGCG could alleviate the degradation of ACAN induced by interleukin-1β (IL-1β) and down-regulated the expression of matrix metalloproteinase (MMP)-1 and MMP-13 in human chondrocytes [19]. However, EGCG possesses limited solubility and is susceptible to air oxidation, resulting in reduced bioavailability and restricted clinical application [20]. The development of nanodrug formulations offers an opportunity to overcome the limitations posed by EGCG monomers [21–23]. Nevertheless, existing techniques, such as polymer coupling and metal coordination, involve complex synthesis processes and the use of templates, which undoubtedly affect the biological activity of polyphenols and increase their potential biological toxicity [24–26]. Consequently, preparing highly bioactive EGCG nanodrugs using green and efficient methods is essential for their effective application.

Small amino acid molecules exhibit notable advantages in constructing nanodrug formulations owing to their diverse variety, well-defined structures, ease of modification, and low immunogenicity [27–29]. Furthermore, certain small amino acid molecules [e.g., selenomethionine (SeMet)] can function as antioxidants and GPX-like redox catalysts, while also supplementing selenium levels, potentially exerting a beneficial effect on the progression of ferroptosis-induced OA [30–32]. This study aimed to devise a rapid and convenient method to prepare an EGCG-based nanodrug (ES ND) in water. The process mainly involved the Mannich condensation reaction between EGCG and SeMet, generating EGCG-SeMet oligomers that subsequently assemble to form ES NDs driven by hydrogen bonding and π-π interactions [33,34]. The physicochemical properties of ES NDs can be regulated by adjusting thermodynamic and kinetic parameters, such as the ratio, concentration, and reaction time of the reactants. The results of our study demonstrate that ES NDs could eliminate ROS accumulation in chondrocytes,
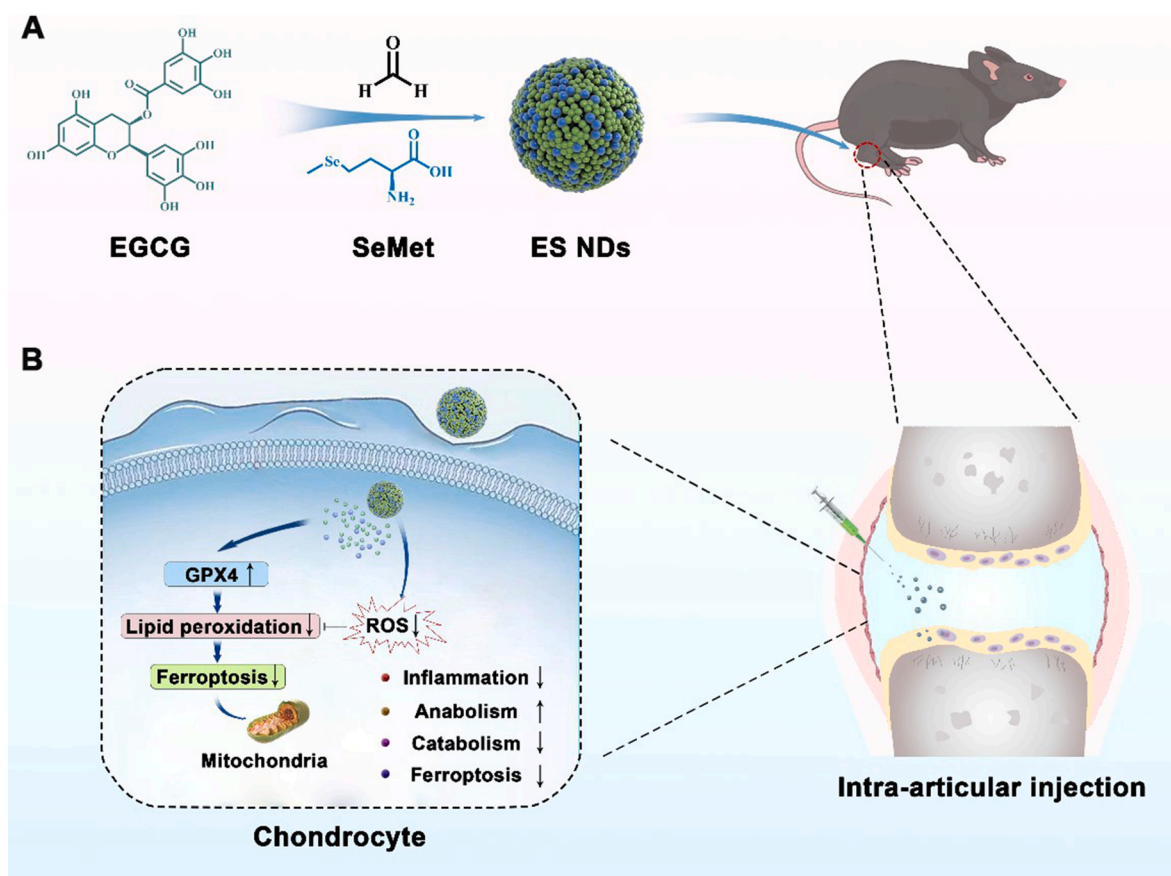
Scheme 1. Schematic illustration of the construction of ES NDs and the treatment of OA. (A) Assembly process of ES NDs. (B) The uptake of ES NDs by chondrocytes mitigates ferroptosis-induced OA.

ameliorate the reduction of GPX4 expression, effectively inhibit the secretion of inflammatory cytokines, and improve the metabolic disorder of chondrocytes, thereby alleviating the OA caused by ferroptosis. *In vivo* research results indicated that ES NDs could be retained within the joint cavity for at least 2 weeks, and substantially enhance the efficacy of OA treatment (Scheme 1). This method showcased a green and facile approach to prepare highly bioactive ES NDs, offering promising prospects for treating OA.

2. Materials and methods

2.1. Materials

EGCG (MB1672) was purchased from Meilun Biotechnology Co., Ltd. (China). SeMet (3211-76-5) was obtained from MedChemExpress Biotechnology (China). 1,1-Diphenyl-2-picrylhydrazyl (DPPH, 1707-75-1) and hydrogen peroxide (H_2O_2, 88,597-100ML-F, 3 wt%) was purchased from Sigma-Aldrich (China). 2′,7′-dichlorodihydrofluorescein diacetate (DCFH-DA, S0033M) was purchased from Beyotime Biotechnology (China). Bovine serum albumin (BSA, A801320) was purchased from Shanghai Macklin Biochemical Technology Co., Ltd. (China). Dulbecco's modled Eagle's medium (DMEM, A4192001), fetal bovine serum (FBS, 16140071), and Hoechst 33342 (H1399) were obtained from Thermo Fisher Scientific (China). Cyanine 5 (Cy5, *R*-H-18281) was obtained from Xian ruixi Biological Technology Co., Ltd. (China).

2.2. Preparation of ES NDs

To prepare ES NDs, EGCG (22.875 mg) and SeMet (3.26 mg) were dissolved in deionized water (10 mL). Then, 7.5 μL of formaldehyde solution (40%) was added to the mixed solution at room temperature (25 °C). The ES NDs were finally obtained by centrifugation (12,000*g*, 5 min) and purification after 5 h of continuous vigorous magnetic stirring in the dark.

2.3. Measurements

A Malvern dynamic laser scattering (DLS) analyzer (NanoZS, UK) was used to measure the size distribution and zeta potential of the ES NDs. Transmission electron microscope (TEM) images of the ES NDs were acquired using a JEOL JEM-1400 TEM (Japan). The ultraviolet–visible (UV–vis) spectra were obtained using a Shimadzu UV-2600 spectrophotometer (Japan). High angle annular dark field (HAADF) and the energy-dispersive X-ray (EDX) spectroscopy elemental mapping images were characterized on a Thermo Scientific Talos F200i TEM (USA) at an operation voltage of 200 kV. The components in ES NDs were quantified using an Agilent 1260 Infinity II (USA) high performance liquid chromatography (HPLC).

2.4. DPPH assays

DPPH free radical scavenging test was performed according to the method described in a previous study [35]. First, stock solutions of DPPH in ethanol (0.1 mM) were freshly prepared and stored in the dark. Then, ES NDs resuspension was added to 4 mL of DPPH solution separately; the EGCG concentration in the mixed solution was 2.5, 5.0, and 10.0 μg mL^{-1}. Then, the mixed solution was placed in a dark place, and absorption was detected at a predetermined time point. The DPPH radical scavenging activity was calculated using the following formula: $S = [1 - (A_m - A_n)/A_0] \times 100\%$, where A_m is the absorbance of the mixture of DPPH and ES ND resuspension, *An* is the absorbance of ES NDs in ethanol solution, and A_0 is the absorbance of DPPH solution without ES NDs. The UV–vis absorption peak at 517 nm was used to calculated the scavenging activity.

2.5. Cell viability

The cell viability was assessed using the Cell Counting Kit-8 (CCK-8) assay kit (CK04, Dojindo, Japan) following the manufacturer's protocols. Briefly, the chondrocytes were seeded into 96-well plates. Then, 10 μL of CCK-8 solution was added per well, and the chondrocytes were incubated for 2 h. The absorbance values at 450 nm were measured using a microplate reader (VARIOSKAN FLASH, Thermo Fisher Scientific, USA).

2.6. Intracellular uptake of ES NDs

Cy5-labeled ES NDs were co-cultured with chondrocytes for 3 h and washed with PBS for three times. The chondrocytes were then fixed with 4% paraformaldehyde (G1101, Servicebio, China) for 15 min and incubated in 0.5% Triton X-100 (T9284, Sigma, USA) for 15 min. After washed again thrice with PBS, the chondrocytes were treated with 100 μM TRITC Phalloidin (CA1610, Solarbio, China) and Hoechst 33342 (diluted 1:1000) for 20 min. Subsequently, high-content screening (Opera Phenix Plus, PerkinElmer, USA) was employed to observe and analyze the chondrocytes. In addition, the chondrocytes were co-cultured with Cy5-labeled ES NDs for 1 h, 3 h, 6 h, 12 h and 24 h, and a BD flow cytometer (FACSCalibur, BD Biosciences, USA) was employed to analyze the fluorescence intensity of Cy5 in chondrocytes.

2.7. Intracellular oxidative stress detection

The human knee cartilage samples were obtained from three female patients (Patient 1: 56-year-old, BMI = 26.04. Patient 2: 60-year-old, BMI = 35.16. Patient 3: 66-year-old, BMI = 30.10) who underwent unilateral total knee arthroplasty at Qilu Hospital of Shandong University due to OA without any concomitant systemic diseases. The cartilage samples from the medial and lateral femoral condyles of patients undergoing total knee arthroplasty were collected and prepared into frozen sections. Subsequently, the cartilage tissue was incubated with a 5 μM Dihydroethidium (DHE) (S0063, Beyotime Biotechnology, China) solution at 37 °C for 30 min, followed by observation under a fluorescence microscope (OLYMPUS, CKX53, Japan).

Briefly, chondrocytes were cultured with H_2O_2 (0.2 mM), H_2O_2 (0.2 mM) + SeMet (89.7 μM), H_2O_2 (0.2 mM) + EGCG (0.11 mM), and H_2O_2 (0.2 mM) + ES NDs (equivalent SeMet concentration of 89.7 μM and EGCG concentration of 0.11 mM) for 12 h. DCFH-DA probe was used to detect the ROS levels in chondrocytes [36]. Then, the chondrocytes were washed thrice with preheated PBS, and the DCFH-DA probe was diluted in serum-free DMEM medium at a ratio of 1:1000 to form the staining solution. After incubated in a 5% CO_2 cell incubator at 37 °C for 30 min, the chondrocytes were washed thrice with a serum-free medium, and observed under a fluorescence microscope (OLYMPUS, CKX53, Japan). The mitochondrial membrane potential of chondrocytes was detected by mitochondrial membrane potential assay kit (C2006, Beyotime Biotechnology, China). Chondrocytes were incubated with JC-1 staining solution at 37 °C for 30 min, followed by three washes using 1*X* JC-1 buffer, and observed under a fluorescence microscope (OLYMPUS, CKX53, Japan). Subsequently, the levels of lipid peroxidation (malondialdehyde, MDA), Fe^{2+} in chondrocytes were detected by the corresponding assay kits (M496 and F374, Dojindo, Japan) according to their manufacturer's instructions, the levels of MDA were measured using a microplate reader (VARIOSKAN FLASH, Thermo Fisher Scientific, USA), Fe^{2+} in chondrocytes observed under a fluorescence microscope (OLYMPUS, CKX53, Japan). The oxygen consumption rate (OCR) of chondrocytes in various treatment groups was performed on Seahorse Instrument (Agilent Technologies, USA).

2.8. Quantitative real-time polymerase chain reaction analysis

Total RNA from each treatment group was extracted using an RNA

extraction kit (RN001, Yishan Biotechnology, China) to determine the RNA concentration of each group. The RNA was reverse-transcribed into cDNA using a reverse transcription kit (RT001, Yishan Biotechnology, China). Quantitative real-time polymerase chain reaction (qRT-PCR) was performed on a 7500 RT-PCR system (Applied Biosystems, USA). The primer nucleotide sequences used in this experiment are presented in Table S1.

2.9. Western blot analysis

Collecting each group of chondrocytes and extracting the total protein from them. After centrifugation at 12,000g for 20 min at 4 °C, the supernatant was decanted and mixed with sample loading buffer at a ratio of 4:1. The mixture was then heated to 100 °C for 10 min. The target proteins were transferred onto a polyvinylidene difluoride (PVDF) membrane (IPVH00010, Millipore, USA), following electrophoresis on a 10% sodium dodecyl sulfate-polyacrylamide gel, blocked with 5% BSA at room temperature for 1 h, and subsequently probed with their corresponding primary antibodies (Table S2). After overnight incubation at 4 °C, the proteins were washed four times with TBS + Tween (TBST) buffer solution for 10 min each. Subsequently, PVDF membranes were incubated with secondary antibodies (ZB-5301, ZSGB-BIO, China) at room temperature for 2 h and washed thrice with TBST for 10 min each time. Finally, the protein content was visualized using a Tancon 5200 automatic chemiluminescence image analysis system (Tancon, China).

2.10. Immunofluorescence staining

Briefly, the chondrocytes were fixed with 4% paraformaldehyde for 20 min, permeabilized using 0.5% Triton X-100 for 15 min, and then blocked with 5% bovine serum albumin (BSA) for 2 h. Subsequently, rabbit primary antibodies against COX-2, SOX9, and GPX4 (Table S2) were diluted at a ratio of 1:100, incubated at a temperature of 4 °C for 12 h. Subsequently, the goat anti-rabbit secondary antibody (GB27303, Servicebio, China) was diluted to a concentration of 1:100 and incubated with the chondrocytes at room temperature for 1 h. The chondrocytes were then stained with 100 μM TRITC Phalloidin and Hoechst 33342 (diluted 1:1000) for 20 min, and finally observed using high-content screening (Opera Phenix Plus, PerkinElmer, USA).

2.11. Destabilization of the medial meniscus (DMM) model of mice

All the animal care and experimental protocols were performed by the Animal Ethical and Experimental Committee of the Chinese PLA General Hospital. Ten-week-old C57BL/6 mice were selected to establish the DMM model. Sodium pentobarbital was administered for complete anesthesia. Then, aseptic preparation was performed on the knee joint, and a 0.8 cm longitudinal incision was made along the medial aspect of the joint. The medial meniscus was meticulously exposed layer by layer, and the medial meniscotibial ligament was incised to create a model of joint instability. The mice were divided into five groups: Control, DMM, EGCG, SeMet, and ES NDs (n = 4). Phosphate buffered saline (PBS, 1x), EGCG, SeMet, and ES NDs were injected into the knee articular cavity of mice biweekly. After 3 months of post-surgery, the knee joints of the mice were harvested for subsequent studies.

2.12. Extraction of chondrocytes from mice

The cartilage tissue was collected from the knee joints of 1-week-old C57 mice under sterile conditions and cut into 0.5 m^3 soft tissue blocks with sterile scissors. The cartilage tissue was digested with 0.25% trypsin (25200–072, Gibco, USA) in a cell incubator containing 5% CO_2 at 37 °C for 15 min. The supernatant was removed by centrifugation and digested with 0.2% collagenase-II (2275MG100, BioFroxx, Germany) in a cell incubator containing 5% CO_2 for 4 h at 37 °C. The cells were filtered using a 100-mesh filter and seeded into cell culture dishes for

further culture and subsequent experiments.

2.13. β-galactosidase staining

β-galactosidase staining was carried out in accordance with the manufacturer's instructions (C0602, Beyotime Biotechnology, China). After the chondrocytes were washed with PBS for three times, 1 mL of β-galactosidase staining fixative was added and the cells were fixed at room temperature for 15 min. Then, cells were washed three times with PBS and 1 mL of staining working solution was added to each well and incubated overnight at 37 °C. Finally, the chondrocytes were observed under an ordinary light microscope (TS2, Nikon, Japan).

2.14. Biodistribution and retention of ES NDs in vivo

Cy5-labeled ES NDs and Cy5 dye alone were separately injected into the knee joints of mice. The fluorescence intensity of Cy5 in the knee joint was monitored using a *in vivo* imaging system (IVIS Spectrum, PerkinElmer, USA) at various time points (0, 3, 5, 7, 10, and 14 days) postinjection.

2.15. Micro computed tomography (CT)

The mice knee specimens were scanned using a Quantum GX Micro CT Imaging System (PerkinElmer, USA) with the following experimental settings: 90 kV X-ray voltage, 80 μA node current, and 1500 ms exposure time for each of the 360 rotational steps. Then, three-dimensional (3D) images were reconstructed using multimodal 3D visualization software.

2.16. Histological staining

After rinsing thrice with precooled PBS, the mice knee joints were fixed with 4% paraformaldehyde for 48 h. Afterward, the mice knee tissues were immersed in a decalcifying solution, and the fresh solution was replenished daily until the joint tissues were sufficiently softened. Subsequently, the joint tissues were embedded in paraffin wax, and trimmed blocks were sectioned using a paraffin microtome. Then, the paraffin sections were placed in an oven at 65 °C for 2 h, deparaffinized with environmentally friendly deparaffinized solution, and washed with absolute ethanol, 75% alcohol and distilled water. Hematoxylin and eosin (H&E) staining was carried out in accordance with the manufacturer's instructions (G1076, Servicebio, China), and observed under a microscope. For Safranin O-Fast Green (SO-FG) staining (G1053, Servicebio, China), the sections were then stained in fast green staining solution, washed with water to remove the excess staining solution, immersed in 1% hydrochloric acid alcohol for 10 s, and immersed in safranin O staining after washing with water. After rapid dehydration with absolute ethanol, the slices were rendered transparent with xylene, sealed, and observed under a microscope. Toluidine blue (TB) staining (G1032, Servicebio, China) was conducted in accordance with the manufacturer's instructions. Briefly, the sections were rinsed with distilled water, immersed in TB staining solution for 5 min, washed with water, cleared with xylene for 5 min, and observed under a microscope.

2.17. Immunohistochemical staining

Briefly, the knee joint tissues were embedded in paraffin, and trimmed wax blocks with a thickness of 4 μm were sectioned using a paraffin microtome for subsequent experimental manipulations. The paraffin-embedded sections were deparaffinized using an environmentally friendly deparaffinization solution. Antigen retrieval was performed using an antigen repair solution, endogenous peroxidase was blocked with 3% H_2O_2, and then 3% BSA was used to block for 1 h at room temperature. The specific rat primary antibodies of ACAN, Col-2, and GPX4 (Table S2) were incubated at a dilution ratio of 1:100 overnight at 4 °C, followed by four washes with PBS for 10 min each. The secondary

antibodies (G1213, GB27303 and G1214, Servicebio, China) were then incubated at room temperature with a dilution ratio of 1:100 for 1 h.

2.18. Statistical analysis

The data were analyzed using GraphPad Prism 8.0 (GraphPad Software Inc., CA, USA). All data were shown as mean ± standard deviation. Comparison between more than two groups was analyzed by one-way analysis of variance followed by Tukey's *post hoc* test. A *P* value < 0.05 indicated a statistically significant difference.

3. Results and discussion

3.1. Preparation and characterization of ES NDs

We synthesized ES NDs by a simple process of adding a trace amount of formaldehyde to the EGCG-SeMet mixed aqueous solution, stirring vigorously at room temperature for 5 h. The ES NDs were then obtained through centrifugation and purification. As illustrated in Fig. 1A, DLS results revealed that the particle size of ES NDs was approximately 175.2 nm with a negative charge of −32.8 mV. TEM image showed that ES NDs exhibited a regularly spherical and had good dispersibility (Fig. 1B). Subsequently, we investigated the formation and growth process of ES NDs with reaction time. As shown in Fig. S1A, large number of small complexes were formed after 2 h of reaction between EGCG and SeMet. These small complexes gradually converged into

larger aggregates (Fig. S1B), and the aggregates assembled into complete spherical ES NDs after 5 h of reaction (Fig. 1B). The formation mechanism of ES NDs can be divided into the following two steps. Firstly, EGCG and SeMet are covalently crosslinked through Mannich condensation reaction to form EGCG-SeMet oligomers [33,34]. Subsequently, these polyphenol-amino acid oligomers were assembled into the complete spherical ES NDs driven by non-covalent interactions such as hydrogen bonding and π-π stacking [37,38]. As illustrated in Fig. 1C and Fig. S2, the size of ES NDs gradually increased as the reaction time prolongs, and the particle size increased to around 1.2 μm at 24 h. At the same time, we monitored the zeta potential of ES NDs and the results demonstrated that the zeta potential remained around −36 to −32 mV with reaction time. As depicted in Fig. 1D, HAADF and EDX mapping images showed that the elements of C, N, O, and Se were uniformly distributed throughout the ES NDs, confirming the successful loading of SeMet. As shown in Fig. 1E, UV–vis spectrum of ES NDs exhibited a characteristic absorption peak at 273 nm, which matched well with that of free EGCG. Combined with the results determined by HPLC, the contents of EGCG and SeMet in ES NDs were determined to be 86.4% and 13.6%, respectively.

As an excellent natural antioxidant, EGCG could effectively eliminate ROS produced by chondrocytes, thereby inhibiting the process of OA. As shown in Fig. 1F, DPPH assay was used to detect the antioxidant activity of ES NDs, and the results proved that the free radical scavenging ability of the ES NDs increased with the increase in EGCG concentration. When the concentration of EGCG in ES NDs reached 10 μg mL^{-1}, the free
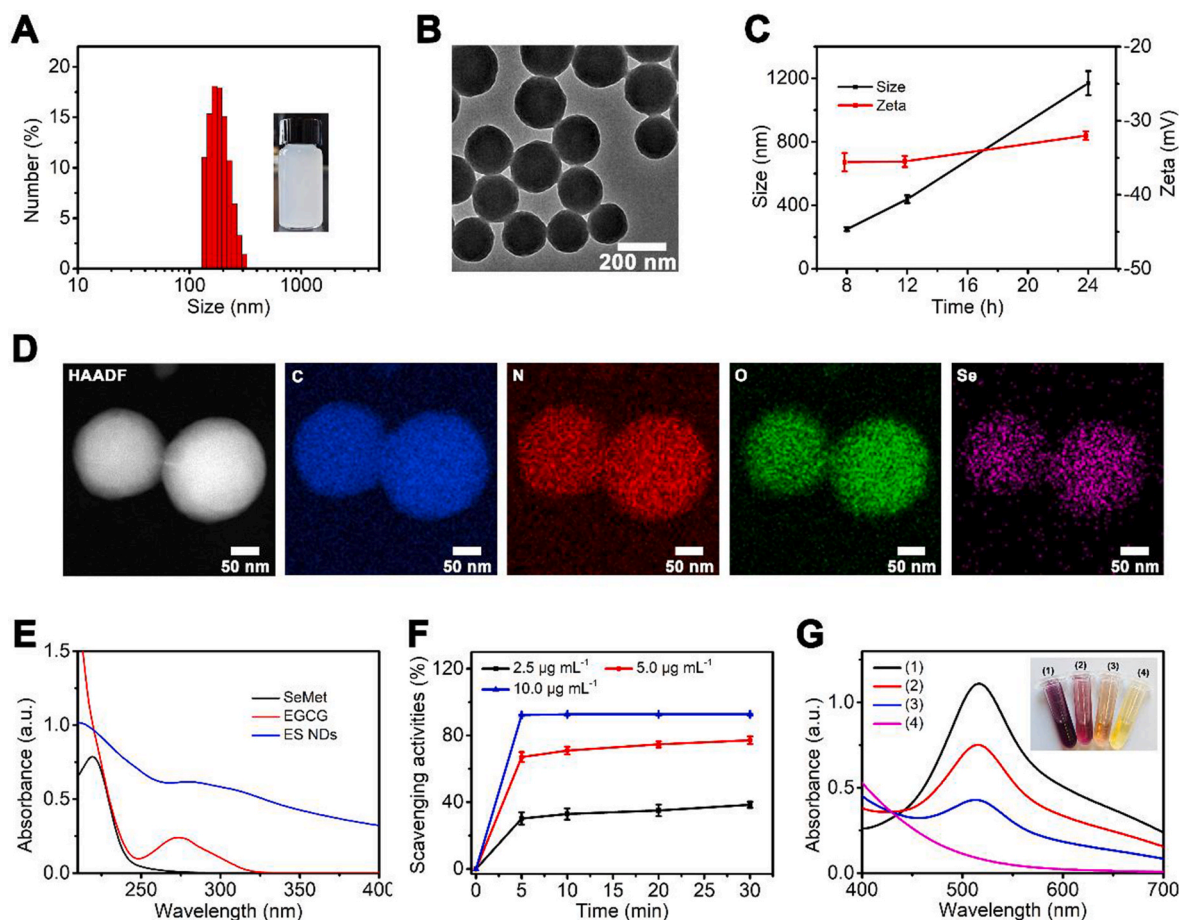

Fig. 1. Physicochemical properties of ES NDs. (A) DLS result of ES NDs, where the inset represents the corresponding resuspension solution. (B) TEM image of the ES NDs. Scar bar: 200 nm. (C) Size and zeta potential variations of ES NDs with reaction time. (D) HAADF and the corresponding EDX spectroscopy elemental mapping images of ES NDs. Scar bar: 50 nm. (E) UV–vis spectra of EGCG, SeMet, and ES NDs. (F) Radical scavenging ability variation with time and ES NDs concentration, the equivalent EGCG concentrations are 2.5, 5.0, and 10.0 μg mL^{-1}, respectively. (G) UV–vis spectra of the DPPH ethanol solution incubated with ES NDs for 30 min, the equivalent EGCG concentrations from (2)–(4) are 2.5, 5.0, and 10.0 μg mL^{-1}, respectively; the inset shows the photograph of the final solutions.

radical scavenging ability reached more over 90%. As shown in Fig. 1G, after co-incubating DPPH with the particles for 30 min, the color of the DPPH solution changed from purple to pale yellow, and the characteristic absorption peak almost completely disappeared. The excellent antioxidant activity of ES NDs also served as the basis for the subsequent inhibition of OA.

3.2. The biocompatibility of ES NDs and their endocytosis by chondrocytes

The state of chondrocytes required for the experiment was first assessed using β-galactosidase staining. Optical image of chondrocytes revealed a predominance of normal cells with only a minor presence of senescent cells, indicating the favorable conditions of chondrocytes (Fig. S3). Then, the impact of ES NDs on chondrocyte viability was evaluated using the CCK-8 assay. As shown in Fig. 2A and 2B, after chondrocytes co-cultured with ES NDs for 24 h and 48 h, the concentrations ranging from 0 to 20 μg mL^{-1} exhibited favorable biocompatibility with negligible cytotoxicity. Therefore, we selected a concentration of 20 μg mL^{-1} for subsequent experiments. As depicted in Fig. 2C, the flow cytometry results demonstrated a gradual increase in both the number of Cy5-positive cells and intracellular fluorescence intensity with prolonged exposure time. This study unequivocally confirmed the ability of chondrocytes to internalize ES NDs, which exhibited an incremental uptake over time. Subsequently, high-content screening was used to observe the uptake ability of ES NDs by chondrocytes. As depicted in Fig. 2D, a significant quantity of Cy5-labeled ES NDs was found to be internalized by chondrocytes within 3 h.

3.3. ES NDs ameliorated H$_2$O$_2$-induced ferroptosis of chondrocytes

GPX4, an essential selenoprotein for cartilage growth, is pivotal in regulating ferroptosis [39,40]. Selenium is closely linked to the expression of GPX4 and can facilitate its transcriptional upregulation [41]. Moreover, a deficiency in selenium may significantly impede the growth of bone and cartilage tissue [42]. Hence, targeting the selenium-GPX4 axis represents a pivotal strategy for ameliorating ferroptosis-driven OA. GPX4 plays a crucial role in conferring resistance to ferroptosis. The depletion of GPX4 significantly elevates intracellular Fe^{2+} levels, which triggers excessive ROS production via the Fenton reaction and ultimately promotes lipid peroxidation [8,14]. Meanwhile, lipid peroxidation can lead to mitochondrial ultrastructure abnormalities, such as reduced mitochondrial volume, increased mitochondrial membrane density, and loss of mitochondrial ridges [45]. These pathological changes further disrupt the functional homeostasis of cartilage tissue, thereby contributing to the development and progression of OA. Therefore, ameliorating various pathological processes that lead to ferroptosis represents a novel approach to alleviating OA. Previous research has demonstrated the potential of EGCG in mitigating diverse pathological processes associated with ferroptosis, whereby it attenuates hepatic lipidtoxicity induced by high-fat diets through targeting mitochondrial ROS-mediated ferroptosis [46]. Previous research has demonstrated that supplementation of SeMet enhances the expression of GPX4 at the cellular level and effectively mitigates the production of lipid ROS [41]. The findings suggest that EGCG and SeMet were effective in reducing ferroptosis, thereby establishing a robust theoretical foundation for employing ES NDs in the treatment of ferroptosis-induced OA.

Before we conducted in vitro experiments to further investigate the pathological changes induced by ROS in chondrocytes, the ROS levels were assessed in chondrocytes derived from OA patients. As shown in Fig. S4, ROS has been detected in chondrocytes in both mild OA (lateral femoral condyle) and relatively severe OA areas (medial femoral condyle), and the ROS levels are higher in relatively severe OA areas. The results demonstrate the presence of ROS in clinical OA specimens and its correlation with OA severity. To evaluate the role of ES NDs in scavenging ROS, intracellular ROS level was measured using DCFH-DA
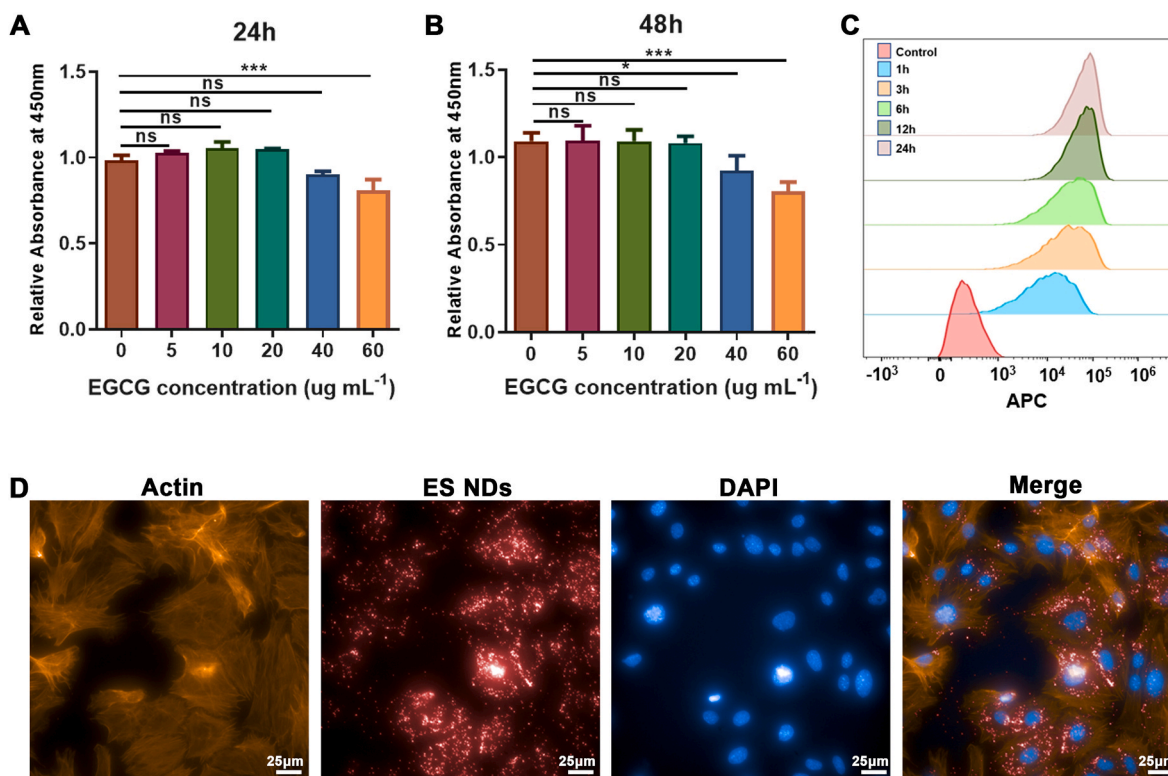

Fig. 2. Cytocompatibility and cellular uptake of ES NDs. (A–B) Cell viability of chondrocytes co-cultured with various concentrations of ES NDs at 24 h and 48 h. (C) Fluorescence intensity of Cy5 in chondrocytes was measured using flow cytometry. (D) High-content screening assay was conducted to evaluate the uptake capacity of chondrocytes for ES NDs. Scale bar: 25 μm ns (no statistical significance), *$P < 0.05$, ***$P < 0.001$.

probe. After H_2O_2 treatment, the ROS (green fluorescence) significantly increased compared with the control group. And the intracellular ROS levels significantly decreased after treatment with EGCG, SeMet, and ES NDs. It is noted that ES NDs had a stronger effect in reducing the ROS levels than SeMet and EGCG (Fig. 3A and 3C). The FerroOrange probe (Fe^{2+} probe) was employed to measure the accumulated Fe^{2+} content in chondrocytes after H_2O_2 treatment. As shown in Fig. 3B and 3D, our findings indicated a significant increase in the abnormal accumulation of Fe^{2+} following H_2O_2 treatment compared with that in the control group. However, the abnormal accumulation of Fe^{2+} in chondrocytes gradually reduced after intervention with EGCG, SeMet, and ES NDs, and the efficacy of ES NDs surpassed that of SeMet and EGCG. We further assessed the extent of lipid peroxidation in chondrocytes induced by H_2O_2 by quantifying the levels of MDA. As shown in Fig. 3E, the expression level of MDA in chondrocytes was significantly elevated following H_2O_2 treatment. However, SeMet failed to attenuate the expression level of MDA, whereas EGCG and ES NDs treatment markedly reduced the expression level of MDA. The reduction in the expression level of MDA was obviously more pronounced following treatment with ES NDs compared with EGCG; however, the difference between the two treatments did not reach statistical significance. This implied that the effectiveness of SeMet in eliminating MDA was limited, and the scavenging activity of ES NDs on MDA was mainly attributed to EGCG. Hence, ES NDs could mitigate H_2O_2-induced ROS and Fe^{2+} accumulation in chondrocytes, as well as attenuate lipid peroxidation elicited by H_2O_2, which was evidenced by a reduction in the expression level of MDA.

We subsequently assessed the involvement of ES NDs in mitigating H_2O_2-induced ferroptosis in chondrocytes by quantifying key ferroptosis markers, including GPX4, ferritin heavy chain 1 (FTH1), acyl-CoA synthetase long-chain family member 4 (ACSL4), and NADPH oxidases 1 (NOX1). As illustrated in Fig. 3F–I, H_2O_2 significantly reduced the mRNA expression levels of ferroptosis protective factors (GPX4 and FTH1), but increased the mRNA expression levels of ferroptosis activators (ACSL4 and NOX1) compared with those in the control group. Treatment with SeMet, EGCG, and ES NDs significantly increased the mRNA expression levels of GPX4 and FTH1, it decreased the mRNA expression levels of ACSL4 and NOX1 in chondrocytes, indicating that SeMet, EGCG, and ES NDs could alleviate the pathological process of ferroptosis. ES NDs exhibited superior efficacy compared with SeMet and EGCG in restoring the reduced levels of GPX4 and FTH1 mRNA expression levels induced by H_2O_2. After treatment with ES NDs, the mRNA expression levels of GPX4 and FTH1 reached their peak compared with SeMet and EGCG. ES NDs exhibited superior efficacy in reducing the mRNA expression levels of ACSL4 and NOX1. However, no significant difference in terms of reducing the mRNA expression level of NOX1 was found between ES NDs and SeMet. Therefore, ES NDs could downregulate ferroptosis-related indicators and upregulate anti-ferroptotic markers. As depicted in Fig. 3J, 3K and 3M, treatment with H_2O_2 significantly decreased the protein expression level of GPX4 in chondrocytes, whereas SeMet, EGCG, and ES NDs treatments led to a significant increase in the expression levels of GPX4. Compared with the EGCG treatment, SeMet and ES NDs treatments resulted in a more pronounced upregulation of the expression level of GPX4. Furthermore, the highest expression level of GPX4 was observed in the ES ND group. JC-1 was used to detect the functional status of mitochondria. As depicted in Fig. 3L and 3N, our study found that the H_2O_2 treatment significantly reduced the mitochondrial membrane potential of chondrocytes compared with that in the control group. However, SeMet, EGCG, and ES NDs intervention significantly improved the loss of mitochondrial membrane potential of chondrocytes. Among these, ES NDs had the best therapeutic effect compared with SeMet and EGCG. Then, the mitochondrial function was further evaluated through the oxygen consumption rate (OCR). The results showed a significant decrease in OCR value of chondrocytes after treatment with H_2O_2. However, the decrease of OCR values was reversed by the treatment with SeMet, EGCG, and ES

NDs. It is worth noting that the OCR values of the EGCG and ES ND group are comparable to that of the control group, proving that EGCG and ES NDs have the superior ability to protect mitochondria function (Fig. S5). As depicted in Fig. S6, the morphological changes of mitochondria in chondrocytes were observed using TEM. Our investigation revealed that chondrocytes exposed to H_2O_2 exhibited mitochondrial atrophy and a decrease or even disappearance of mitochondrial ridges, which could be ameliorated by ES NDs intervention. Based on the aforementioned experiments, it was inferred that ES NDs exerted a dual pharmacological effect in attenuating H_2O_2-induced ferroptosis of chondrocytes. Specifically, chondrocytes were capable of internalizing ES NDs and subsequently releasing EGCG and SetMet. ES NDs containing SeMet and EGCG demonstrated robust resistance against various pathological processes leading to ferroptosis, primarily by upregulating the expression of proteins that are resistant to ferroptosis and eliminating pathogenic factors associated with ferroptosis. This included rescuing the decreased expression of anti-ferroptotic markers (GPX4 and FTH1), inhibiting the increased expression of pro-ferroptotic markers (ACSL4 and NOX1), decrease the intracellular ROS levels generated in chondrocytes under conditions of oxidative stress, and alleviating Fe^{2+} accumulation, thereby decreasing MDA expression level and maintaining mitochondrial function homeostasis.

3.4. ES NDs ameliorated the inflammatory response and metabolic dysregulation of chondrocytes induced by H_2O_2

Previous studies have demonstrated that iron overload in chondrocytes leads to elevated intracellular levels of ROS and downregulation of GPX4, thereby enhancing the susceptibility of chondrocytes to oxidative stress [47,48]. This process stimulates the secretion of inflammatory mediators, such as IL-1β, and matrix metalloproteinases like MMP13, exacerbating extracellular matrix degradation and accelerating OA progression, therefore, the inhibition of chondrocyte ferroptosis serves as a crucial approach to mitigate chondrocyte inflammation and alleviate OA [10]. As illustrated in Fig. 4A–E, H_2O_2 upregulated the mRNA expression of inflammatory cytokines COX-2, IL-6, and iNOS, as well as ADAMTS-5 and MMP-13. However, treatment with SeMet, EGCG, and ES NDs significantly attenuated the mRNA levels of COX-2, IL-6, iNOS, ADAMTS-5, and MMP-13. Specifically, ES NDs exhibited a statistically significant reduction in the COX-2 mRNA expression levels compared with both EGCG and SeMet, and the efficacy of ES NDs in reducing iNOS mRNA expression level was found to be superior to that of SeMet. Although all three compounds (SeMet, EGCG, and ES NDs) significantly decreased the mRNA expression level of IL-6, no statistically significant difference was found among them. What counts is ES NDs exhibited significant advantages in reducing the expression levels of ADAMTS-5 and MMP-13 compared with SeMet and EGCG. SOX9 is a pivotal transcription factor that governs chondrogenesis and facilitates the expression of Col-2 and ACAN [49]. Therefore, it is crucial in the maintenance of cartilage matrix homeostasis. As shown in Fig. 4F, H_2O_2 significantly downregulated the expression of SOX-9, while SeMet, EGCG, and ES NDs largely reverse this change. Subsequently, we detected the intracellular immunofluorescence of COX-2 and SOX9 by the high-content screening imaging. As shown in Fig. 4G and 4I, the fluorescence of COX-2 in chondrocytes treated with H_2O_2 was significantly enhanced, but the fluorescence intensity was effectively attenuated by SeMet, EGCG, and ES NDs. And ES NDs exhibited superior efficacy over SeMet and EGCG in suppressing the expression of COX-2. As shown in Fig. 4H and 4J, we observed a significant decrease in the fluorescence intensity of SOX9 upon administration of H_2O_2, while SeMet, EGCG and ES NDs treatments gradually increased SOX9 expression. And ES NDs exhibited superior efficacy compared to EGCG. Although the expression level of SOX9 was higher in the ES ND group than that in the SeMet group, there was no statistically significant difference between these two groups. To further validate the impact of ES NDs on mitigating the inflammatory response and
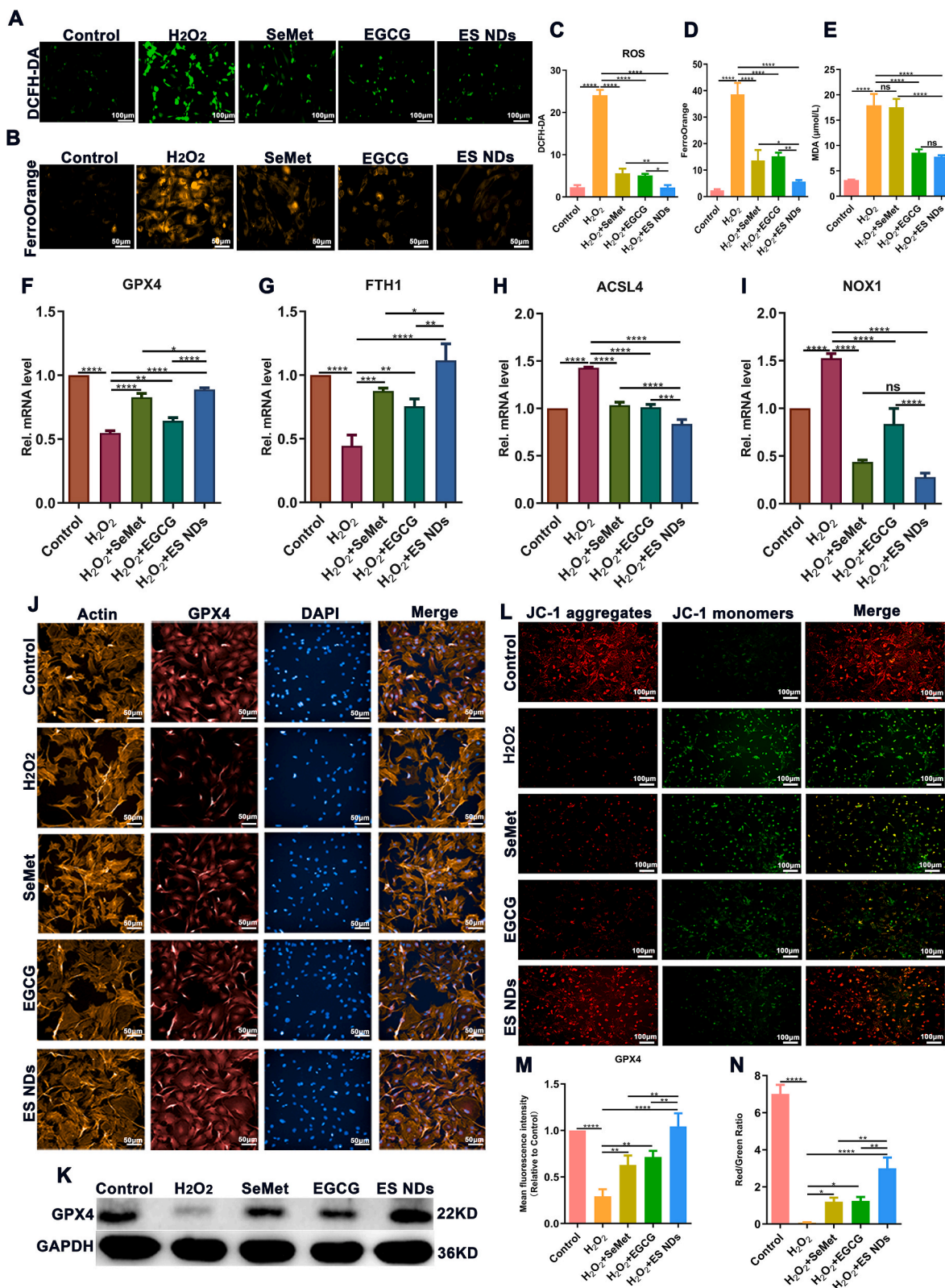
Fig. 3. ES NDs alleviate ferroptosis induced by oxidative stress. (A and C) DCFH-DA probe was used to quantify the level of ROS expression in chondrocytes. Scale bar: 100 μm. (B and D) FerroOrange probe was used to quantify the level of Fe^{2+} expression in chondrocytes. Scale bar: 50 μm. (E) MDA expression levels in each group were quantified using a microplate reader. (F–I) The mRNA expression levels of GPX4, FTH1, ACSL4, and NOX1 were quantified using qRT-PCR analysis. (J) Immunofluorescence and (M) mean fluorescence intensity of GPX4 was assessed via high-content screening. Scale bar: 50 μm. (K) Protein expression level of GPX4 was assessed by Western blot analysis. (L and N) Membrane potential of chondrocyte mitochondria was assessed by means of the JC-1 assay. Scale bar: 100 μm ns (no statistical significance), *P < 0.05, **P < 0.01, ***P < 0.001, ****P < 0.0001.
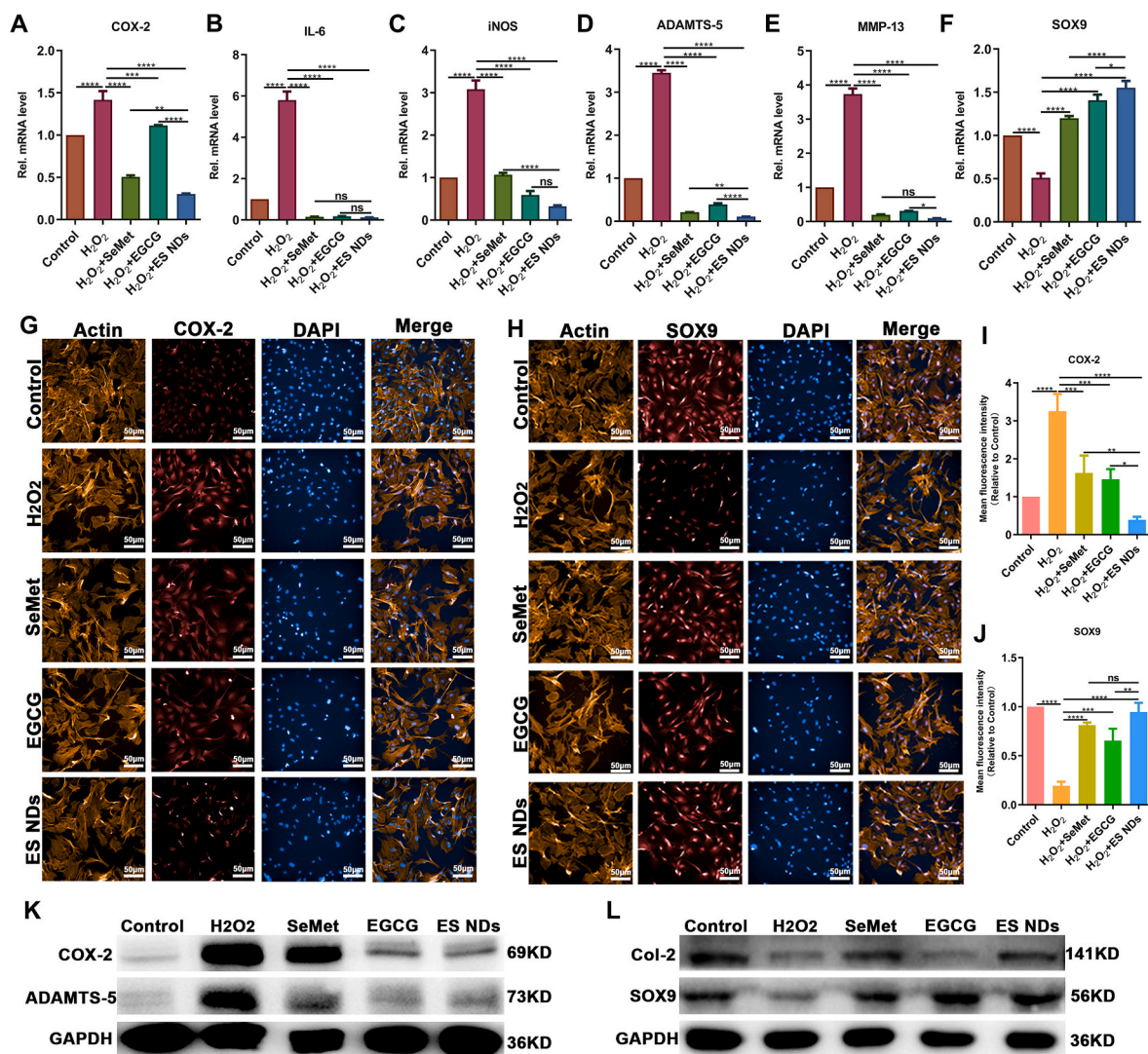
Fig. 4. ES NDs demonstrated efficacy in attenuating inflammation and ameliorating metabolic disorders. (A–F) The mRNA expression levels of COX-2, IL-6, iNOS, ADAMTS-5, MMP-13, and SOX9 were quantified using qRT-PCR analysis. (G, H) Immunofluorescence and (I, J) mean fluorescence intensity of COX-2 and SOX9 were assessed via high-content screening, respectively. Scale bar: 50 μm. (K) Protein expression levels of COX-2 and ADAMTS-5 were assessed by Western blot analysis. (L) Protein expression levels of Col-2 and SOX9 were assessed by Western blot analysis. ns (no statistical significance), $*P < 0.05$, $**P < 0.01$, $***P < 0.001$, $****P < 0.0001$.

ameliorating the metabolic disorder of chondrocytes, the protein expression levels of COX-2, ADAMTS-5, Col-2, and SOX9 were assessed via Western blot analysis. As shown in Fig. 4K, the protein levels of COX-2 and ADAMTS-5 induced by H_2O_2 were significantly inhibited by SeMet, EGCG, and ES NDs. The ES NDs exhibited the highest efficacy in suppressing the expression levels of COX-2 and ADAMTS-5. Compared with SeMet and EGCG, ES NDs exhibited significant advantages in mitigating the H_2O_2-induced decrease in SOX9 and Col-2 protein expression levels, indicating that ES NDs effectively maintained cartilage matrix homeostasis (Fig. 4L). The findings suggest that ES NDs exert a significant impact on mitigating the inflammatory response of chondrocytes, alleviating the metabolic disorders of chondrocytes, reducing the expression levels of pro-catabolic enzymes, and alleviating the depletion of major components of cartilage. Moreover, they offer notable advantages over SeMet or EGCG alone.

3.5. Imaging assessment of the impact of ES NDs on OA in mice using the DMM model

To assess the retention of ES NDs in the knee joint, Cy5 dye alone and Cy5-labeled ES NDs were intra-articularly injected into the knee joint of both groups of mice, and the duration of treatment was determined by monitoring the fluorescence signal intensity. As shown in Fig. 5A and 5B, the fluorescence signal in the knee joint of mice in the Cy5 dye group exhibited a rapid decline and nearly vanished by the 10th day. However, the knee joints of mice still exhibited a visible fluorescence signal and maintained a persistent fluorescence intensity until the 14th day after treatment with Cy5-labeled ES NDs. The results demonstrated the excellent joint retention ability of ES NDs and provided a reference for the interval time of drug administration. We subsequently developed a DMM model to assess the efficacy of ES NDs in ameliorating OA in mice. As shown in Fig. 5C and 5E, the micro-CT results of the knee joint revealed that the PBS group exhibited severe articular deformation, a significant increase in medial osteophytes, notable narrowing of joint space, and marked subchondral bone sclerosis compared with the control group. These findings provided the successful construction of OA model in mice. As depicted in Fig. 5D and 5F, mice treated with SeMet, EGCG, and ES NDs showed a significant reduction in the number and volume of osteophytes in the knee joint, an increase in joint space, and an improvement in subchondral bone sclerosis within the knee joint.
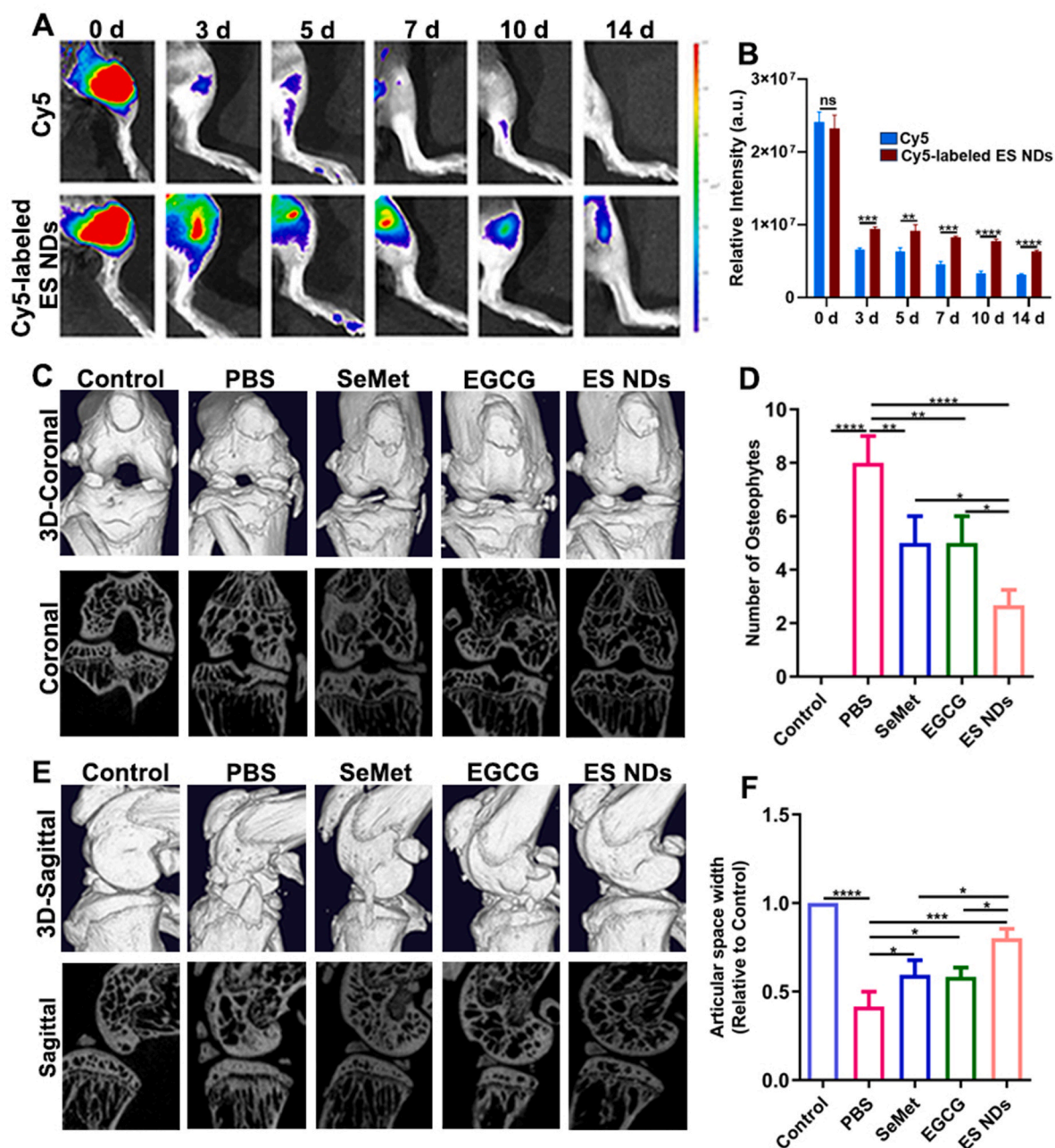
Fig. 5. *In vivo* retention and therapeutic efficacy of ES NDs. (A) Representative fluorescence images and (B) fluorescence intensity of Cy5 dye and Cy5-labeled ES NDs in the knee joint. (C) Representative coronal and (E) sagittal CT images of the knee joint from each experimental group. (D) Number of articular osteophytes in each group. (F) Relative articular space width of the knee joint. ns (no statistical significance), *$P < 0.05$, **$P < 0.01$, ***$P < 0.001$, ****$P < 0.0001$.

Furthermore, the ES ND group exhibited significantly superior outcomes compared with both the EGCG and SeMet groups. This demonstrated that ES NDs were a more effective treatment for OA than either EGCG or SeMet monotherapy, highlighting their potential to enhance treatment efficacy through synergistic effects.

3.6. *In vivo study of ES NDs for alleviating OA in mice*

We conducted histological staining of cartilage tissue using H&E, SO-FG, and TB staining on cartilage tissue to further confirm the effectiveness of ES NDs in alleviating OA in mice. As illustrated in Fig. 6A, the histological examination of mice knee joints revealed that the PBS group exhibited severe OA compared with the control group, characterized by extensive full-thickness injury of knee cartilage, discontinuity and erosion of cartilage surface, significant wear of articular cartilage,

marked reduction in normal chondrocyte count, and exposure of sub-chondral bone. EGCG, SeMet, and ES NDs exhibited a certain therapeutic effect on OA compared with that in the PBS group. The SeMet and EGCG groups exhibited only a limited degree of cartilage damage, with a slight reduction in the number of normal chondrocytes. On the contrary, the ES ND group exhibited smooth articular cartilage without any apparent damage and a normal number of articular chondrocytes. As shown in Fig. 6B and 6C, the results of SO-FG and TB staining indicated that the PBS group had more severe articular cartilage damage, significant depletion of proteoglycan components, and exposure of sub-chondral bone. However, the pathological changes were significantly improved after treatment with SeMet, EGCG, and ES NDs. Following SeMet and EGCG treatment, only localized loss of proteoglycan components was observed in the articular cartilage tissue. The SeMet group exhibited a wider range of proteoglycan component loss compared with
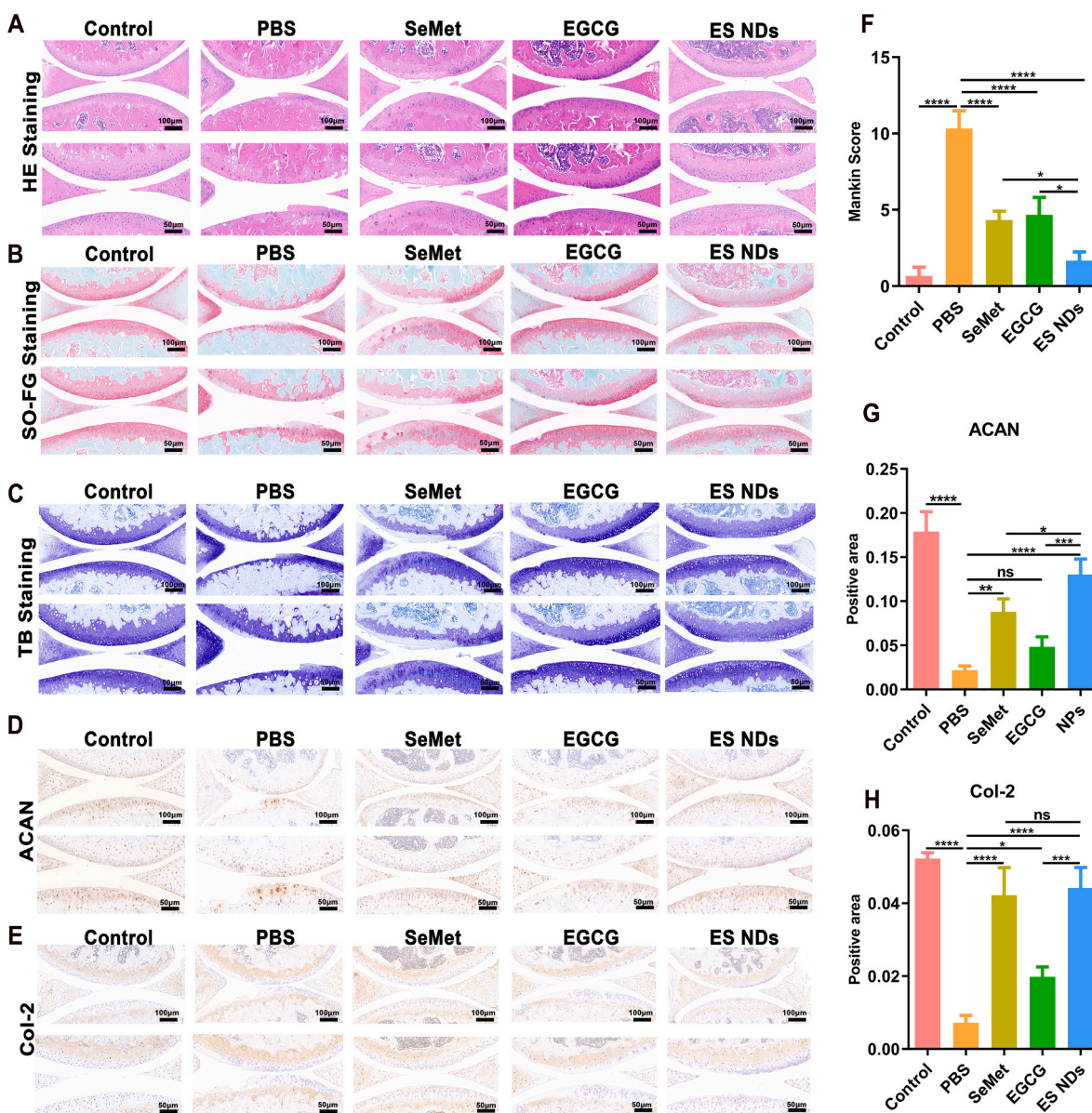
Fig. 6. Histological evaluation of the therapeutic effect of ES NDs on OA. (A) Morphology of the knee joint of mice was detected by H&E staining. Scale bar: 100 μm (low field) and 50 μm (high field). (B) SO-FG staining was employed to identify the proteoglycan composition of knee joints in mice. Scale bar: 100 μm (low field) and 50 μm (high field). (C) TB staining was employed to identify the cartilage matrix constituents in the knee joint of mice. Scale bar: 100 μm (low field) and 50 μm (high field). (D and G) Expression level of ACAN in articular cartilage was assessed via IHC staining. Scale bar: 100 μm (low field) and 50 μm (high field). (E and H) Expression level of Col-2 in articular cartilage was assessed via IHC staining. Scale bar: 100 μm (low field) and 50 μm (high field). (F) Mankin score in different groups. ns (no statistical significance), *$P < 0.05$, **$P < 0.01$, ***$P < 0.001$, ****$P < 0.0001$.

the EGCG group, but with a smoother articular cartilage surface. Both the SeMet and EGCG groups displayed partial cracks on the articular surface and thinning of the articular cartilage layer. However, only a minor reduction in proteoglycan content was detected in the ES ND group, and no visible crack or subchondral bone exposure was observed on the smooth surface of the articular cartilage. After the intervention of ES NDs, a remarkable enhancement was observed in articular cartilage regarding matrix staining, morphological alterations, and overall integrity. Notably, the cartilage surface exhibited a smoother appearance accompanied by intensified proteoglycan staining. Based on the results of histopathological staining, the severity of OA was subsequently evaluated using the Mankin score. As depicted in Fig. 6F, the PBS group demonstrated significantly higher scores compared with the other groups, indicating a more severe manifestation of OA. After treatment with SeMet, EGCG, and ES NDs, the Mankin score gradually

decreased, indicating the efficacy of SeMet, EGCG, and ES NDs in alleviating OA. The ES ND group demonstrated a significantly lower Mankin score compared with the other two groups, indicating that ES NDs possessed superior therapeutic efficacy for OA. IHC staining was performed to assess the expression levels of Col-2 and ACAN in articular cartilage. As depicted in Fig. 6D and 6E, 6G and 6H, the expression of Col-2 significantly diminished in the PBS group. However, the SeMet, EGCG, and ES ND groups exhibited remarkable efficacy in mitigating Col-2 degradation compared with the PBS group. The content of Col-2 significantly increased in the SeMet, EGCG, and ES ND groups compared with the PBS group. The ES ND group showed a significantly higher Col-2 content than the EGCG group, but no significant difference was observed between the ES ND and SeMet groups. In addition to EGCG, both SeMet and ES NDs demonstrated significant advantages in alleviating ACAN loss, with the effect of ES NDs being significantly

better than that of the SeMet.

Immunofluorescence staining was employed to assess the expression level of GPX4 in the knee joint of mice. As depicted in Fig. S7A and S7B, a significant reduction in GPX4 expression was observed within the knee cartilage of PBS group compared with control group. Although EGCG could elevate the expression level of GPX4, no statistically significant difference was observed compared with PBS. The deletion of GPX4 was significantly ameliorated by both SeMet and ES NDs, with SeMet demonstrating superior therapeutic efficacy, although without statistical significance compared to the ES ND group. As shown in Fig. S8, the biosafety of EGCG, SeMet, and ES NDs was demonstrated through a histological examination using H&E staining of major organs in mice. Our *in vivo* experiments fully demonstrated the efficacy of ES NDs in treating OA, as evidenced by their ability to mitigate the loss of major components of articular cartilage, maintain joint morphology, and extend treatment duration through sustained release. Furthermore, the ES NDs exhibited favorable biosafety.

4. Conclusion

Taken collectively, we report the strategy for the treatment of OA by inhibiting the inflammatory response and metabolic disorder caused by ferroptosis. The ES NDs prepared through a green and efficient strategy maximize the biological activity of each component. ES NDs enhances the therapeutic effects on OA by mitigating oxidative stress-induced ferroptosis, attenuating chondrocyte inflammatory response, suppressing cartilage catabolism, and promoting cartilage anabolism, thereby maintaining the metabolic homeostasis of cartilage. *In vivo* experiments have confirmed that ES NDs can effectively alleviate OA, and have good biological safety, thus proving that the potential efficacy of ES NDs in the treatment of OA is promising. Our research strongly supported the potential of ES NDs in alleviating ferroptosis-induced OA, offering a promising strategy for the development of novel therapeutic options.

Ethics approval and consent to participate

The patients participating in the study provided informed consent, and the study was approved by the Medical Ethical Committee of Qilu Hospital of Shandong University in accordance with medical ethics regulations (KYLI-2020(KS)-624). All the animal care and experimental protocols were performed by the Animal Ethical and Experimental Committee of the Chinese PLA General Hospital (SQ2023613).

Declaration of competing interest

The authors declare no conflict of interest.

CRediT authorship contribution statement

Haichao Yu designed the experiments, drafted the manuscript and cover letter, and analyzed the data performed the cell experiments conducted the animal experiments, Yunpeng Zhao designed the experiments, drafted the manuscript and cover letter, and analyzed the data, Xuhui Zhou designed the experiments, drafted the manuscript and cover letter, and analyzed the data, Haifeng Sun designed the experiments, drafted the manuscript and cover letter, analyzed the data, and synthesized ES NDs, Xuesong Zhang designed the experiments, drafted the manuscript and cover letter, and analyzed the data. Zelong Song performed the cell experiments, Jie Yu performed the cell experiments, Chengqi Jia performed the cell experiments, Boyuan Ren performed the cell experiments. Zhen Zhang conducted the animal experiments, Yuan Dong conducted the animal experiments, Yonggang You conducted the animal experiments.

Appendix A. Supplementary data

Supplementary data to this article can be found online at https://doi.org/10.1016/j.bioactmat.2023.09.020.

References

[1] Q. Yao, X. Wu, C. Tao, W. Gong, M. Chen, M. Qu, Y. Zhong, T. He, S. Chen, G. Xiao, Osteoarthritis: pathogenic signaling pathways and therapeutic targets, Signal Transduct. Target. Ther. 8 (1) (2023) 56, https://doi.org/10.1038/s41392-023-01330-w.

[2] J.G. Quicke, P.G. Conaghan, N. Corp, G. Peat, Osteoarthritis year in review 2021: epidemiology & therapy, Osteoarthr. Cartilage 30 (2) (2022) 196–206, https://doi.org/10.1016/j.joca.2021.10.003.

[3] J. Lo, L. Chan, S. Flynn, A systematic review of the incidence, prevalence, costs, and activity and work limitations of amputation, osteoarthritis, rheumatoid arthritis, back pain, multiple sclerosis, spinal cord injury, stroke, and traumatic brain injury in the United States: a 2019 update, Arch. Phys. Med. Rehabil. 102 (1) (2021) 115–131, https://doi.org/10.1016/j.apmr.2020.04.001.

[4] J.N. Katz, K.R. Arant, R.F. Loeser, Diagnosis and treatment of hip and knee osteoarthritis: a review, JAMA 325 (6) (2021) 568–578, https://doi.org/10.1001/jama.2020.22171.

[5] J. Martel-Pelletier, A.J. Barr, F.M. Cicuttini, P.G. Conaghan, C. Cooper, M. B. Goldring, S.R. Goldring, G. Jones, A.J. Teichtahl, J.P. Pelletier, Osteoarthritis. Nat. Rev. Dis. Primers 2 (2016), 16072, https://doi.org/10.1038/nrdp.2016.72.

[6] X. Li, B. Dai, J. Guo, L. Zheng, Q. Guo, J. Peng, J. Xu, L. Qin, Nanoparticle-cartilage interaction: pathology-based intra-articular drug delivery for osteoarthritis therapy, Nano-Micro Lett. 13 (1) (2021) 149, https://doi.org/10.1007/s40820-021-00670-y.

[7] C. Zeng, N.E. Lane, D.J. Hunter, J. Wei, H.K. Choi, T.E. McAlindon, H. Li, N. Lu, G. Lei, Y. Zhang, Intra-articular corticosteroids and the risk of knee osteoarthritis progression: results from the osteoarthritis initiative, Osteoarthr. Cartilage 27 (6) (2019) 855–862, https://doi.org/10.1016/j.joca.2019.01.007.

[8] L. Tong, H. Yu, X. Huang, J. Shen, G. Xiao, L. Chen, H. Wang, L. Xing, D. Chen, Current understanding of osteoarthritis pathogenesis and relevant new approaches, Bone Res. 10 (1) (2022) 60, https://doi.org/10.1038/s41413-022-00226-9.

[9] L.A. Mandl, Osteoarthritis year in review 2018: clinical, Osteoarthr. Cartilage 27 (3) (2019) 359–364, https://doi.org/10.1016/j.joca.2018.11.001.

[10] Q. Ru, Y. Li, W. Xie, Y. Ding, L. Chen, G. Xu, Y. Wu, F. Wang, Fighting age-related orthopedic diseases: focusing on ferroptosis, Bone Res. 11 (1) (2023) 12, https://doi.org/10.1038/s41413-023-00247-y.

[11] B.R. Stockwell, A.J. Friedmann, H. Bayir, A.I. Bush, M. Conrad, S.J. Dixon, S. Fulda, S. Gascon, S.K. Hatzios, V. Kagan, K. Noel, X. Jiang, A. Linkermann, M. E. Murphy, M. Overholtzer, A. Oyagi, G.C. Pagnussat, J. Park, Q. Ran, C. S. Rosenfeld, K. Salnikow, D. Tang, F.M. Torti, S.V. Torti, S. Toyokuni, K. A. Woerpel, D. Zhang, Ferroptosis: a regulated cell death nexus linking metabolism, redox biology, and disease, Cell 171 (2) (2017) 273–285, https://doi.org/10.1016/j.cell.2017.09.021.

[12] X. Jiang, B.R. Stockwell, M. Conrad, Ferroptosis: mechanisms, biology and role in disease, Nat. Rev. Mol. Cell Biol. 22 (4) (2021) 266–282, https://doi.org/10.1038/s41580-020-00324-8.

[13] Y. Zhang, X. Huang, B. Qi, C. Sun, K. Sun, N. Liu, L. Zhu, X. Wei, Ferroptosis and musculoskeletal diseases: "Iron Maiden" cell death may be a promising therapeutic target, Front. Immunol. 13 (2022), 972753, https://doi.org/10.3389/fimmu.2022.972753.

[14] J. Zheng, M. Conrad, The metabolic underpinnings of ferroptosis, Cell Metabol. 32 (6) (2020) 920–937, https://doi.org/10.1016/j.cmet.2020.10.011.

[15] Y. Ju, H. Liao, J.J. Richardson, J. Guo, F. Caruso, Nanostructured particles assembled from natural building blocks for advanced therapies, Chem. Soc. Rev. 51 (11) (2022) 4287–4336, https://doi.org/10.1039/d1cs00343g.

[16] Y. Guo, Q. Sun, F.G. Wu, Y. Dai, X. Chen, Polyphenol-containing nanoparticles: synthesis, properties, and therapeutic delivery, Adv. Mater. 33 (22) (2021), e2007356, https://doi.org/10.1002/adma.202007356.

[17] B.N. Singh, S. Shankar, R.K. Srivastava, Green tea catechin, epigallocatechin-3-gallate (EGCG): mechanisms, perspectives and clinical applications, Biochem. Pharmacol. 82 (12) (2011) 1807–1821, https://doi.org/10.1016/j.bcp.2011.07.093.

[18] H. Li, D. Xiang, C. Gong, X. Wang, L. Liu, Naturally derived injectable hydrogels with ROS-scavenging property to protect transplanted stem cell bioactivity for osteoarthritic cartilage repair, Front. Bioeng. Biotechnol. 10 (2022), 1109074, https://doi.org/10.3389/fbioe.2022.1109074.

[19] S. Ahmed, N. Wang, M. Lalonde, V.M. Goldberg, T.M. Haqqi, Green tea polyphenol epigallocatechin-3-gallate (EGCG) differentially inhibits interleukin-1 beta-induced expression of matrix metalloproteinase-1 and -13 in human chondrocytes, J. Pharmacol. Exp. Therapeut. 308 (2) (2004) 767–773, https://doi.org/10.1124/jpet.103.059220.

[20] Z. Yi, Z. Sun, G. Chen, H. Zhang, X. Ma, W. Su, X. Cui, X. Li, Size-controlled, colloidally stable and functional nanoparticles based on the molecular assembly of green tea polyphenols and keratins for cancer therapy, J. Mater. Chem. B 6 (9) (2018) 1373–1386, https://doi.org/10.1039/c7tb03293e.

[21] Z. Li, Z. Chen, H. Chen, K. Chen, W. Tao, X. Ouyang, L. Mei, X. Zeng, Polyphenol-based hydrogels: pyramid evolution from crosslinked structures to biomedical applications and the reverse design, Bioact. Mater. 17 (2022) 49–70, https://doi.org/10.1016/j.bioactmat.2022.01.038.

[22] Y. Qu, R. De Rose, C.J. Kim, J. Zhou, Z. Lin, Y. Ju, S.K. Bhangu, C. Cortez-Jugo, F. Cavalieri, F. Caruso, Supramolecular polyphenol-DNA microparticles for in vivo adjuvant and antigen co-delivery and immune stimulation, Angew. Chem. Int. Ed. 62 (12) (2023), e202214935, https://doi.org/10.1002/anie.202214935.

[23] H. Chen, L. Guo, J. Ding, W. Zhou, Y. Qi, A general and efficient strategy for gene delivery based on tea polyphenols intercalation and self-polymerization, Adv. Sci. (2023), e2302620, https://doi.org/10.1002/advs.202302620.

[24] J. Zhou, Z. Lin, Y. Ju, M.A. Rahim, J.J. Richardson, F. Caruso, Polyphenol-mediated assembly for particle engineering, Acc. Chem. Res. 53 (7) (2020) 1269–1278, https://doi.org/10.1021/acs.accounts.0c00150.

[25] Y. Han, R. Lafleur, J. Zhou, W. Xu, Z. Lin, J.J. Richardson, F. Caruso, Role of molecular interactions in supramolecular polypeptide-polyphenol networks for engineering functional materials, J. Am. Chem. Soc. 144 (27) (2022) 12510–12519, https://doi.org/10.1021/jacs.2c05052.

[26] J. Zhou, Z. Lin, M. Penna, S. Pan, Y. Ju, S. Li, Y. Han, J. Chen, G. Lin, J.J. Richardson, I. Yarovsky, F. Caruso, Particle engineering enabled by polyphenol-mediated supramolecular networks, Nat. Commun. 11 (1) (2020) 4804, https://doi.org/10.1038/s41467-020-18589-0.

[27] R. Chang, L. Zhao, R. Xing, J. Li, X. Yan, Functional chromopeptide nanoarchitectonics: molecular design, self-assembly and biological applications, Chem. Soc. Rev. 52 (8) (2023) 2688–2712, https://doi.org/10.1039/d2cs00675h.

[28] C. Overby, S. Park, A. Summers, D. Benoit, Zwitterionic peptides: tunable next-generation stealth nanoparticle modifications, Bioact. Mater. 27 (2023) 113–124, https://doi.org/10.1016/j.bioactmat.2023.03.020.

[29] Y. Liu, R. Chang, R. Xing, X. Yan, Bioactive peptide nanodrugs based on supramolecular assembly for boosting immunogenic cell death-induced cancer immunotherapy, Small Methods 7 (5) (2023), e2201708, https://doi.org/10.1002/smtd.202201708.

[30] Y.R. Seo, C. Sweeney, M.L. Smith, Selenomethionine induction of DNA repair response in human fibroblasts, Oncogene 21 (23) (2002) 3663–3669, https://doi.org/10.1038/sj.onc.1205468.

[31] J. Kohrle, Selenium in endocrinology-selenoprotein-related diseases, population studies, and epidemiological evidence, Endocrinology 162 (2) (2021), https://doi.org/10.1210/endocr/bqaa228.

[32] J.E. Spallholz, Selenomethionine and methioninase: selenium free radical anticancer activity, Methods Mol. Biol. (2019) 199–210, https://doi.org/10.1007/978-1-4939-8796-2_15, 1866.

[33] Z. Yi, G. Chen, X. Chen, X. Ma, X. Cui, Z. Sun, W. Su, X. Li, Preparation of strong antioxidative, therapeutic nanoparticles based on amino acid-induced ultrafast assembly of tea polyphenols, ACS Appl. Mater. Interfaces 12 (30) (2020) 33550–33563, https://doi.org/10.1021/acsami.0c10282.

[34] Z. Yi, X. Chen, G. Chen, Z. Deng, Q. Tong, Z. Sun, X. Ma, W. Su, L. Ma, Y. Ran, X. Li, General nanomedicine platform by solvent-mediated disassembly/reassembly of scalable natural polyphenol colloidal spheres, ACS Appl. Mater. Interfaces 12 (34) (2020) 37914–37928, https://doi.org/10.1021/acsami.0c11650.

[35] G. Lin, M.A. Rahim, M.G. Leeming, C. Cortez-Jugo, Q.A. Besford, Y. Ju, Q. Zhong, S.T. Johnston, J. Zhou, F. Caruso, Selective metal-phenolic assembly from complex multicomponent mixtures, ACS Appl. Mater. Interfaces 11 (19) (2019) 17714–17721, https://doi.org/10.1021/acsami.9b04195.

[36] J. Su, F. Yan, L. Wang, H. Yu, Z. Yan, J. Wei, K. Vasile, X. Zhan, X. Liu, Y. Zhao, Delivery of coenzyme Q10 loaded micelle targets mitochondrial ROS and enhances efficiency of mesenchymal stem cell therapy in intervertebral disc degeneration, Bioact. Mater. 23 (2023) 247–260, https://doi.org/10.1016/j.bioactmat.2022.10.019.

[37] R. Xing, C. Yuan, W. Fan, X. Ren, X. Yan, Biomolecular glass with amino acid and peptide nanoarchitectonics, Sci. Adv. 9 (11) (2023) d8105, https://doi.org/10.1126/sciadv.add8105.

[38] R. Xing, Q. Zou, C. Yuan, L. Zhao, R. Chang, X. Yan, Self-Assembling endogenous biliverdin as a versatile near-infrared photothermal nanoagent for cancer theranostics, Adv. Mater. 31 (16) (2019), e1900822, https://doi.org/10.1002/adma.201900822.

[39] Y. Miao, Y. Chen, F. Xue, K. Liu, B. Zhu, J. Gao, J. Yin, C. Zhang, G. Li, Contribution of ferroptosis and GPX4's dual functions to osteoarthritis progression, EBioMedicine 76 (2022), 103847, https://doi.org/10.1016/j.ebiom.2022.103847.

[40] T.M. Seibt, B. Proneth, M. Conrad, Role of GPX4 in ferroptosis and its pharmacological implication, Free Radic. Biol. Med. 133 (2019) 144–152, https://doi.org/10.1016/j.freeradbiomed.2018.09.014.

[41] Y. Yao, Z. Chen, H. Zhang, C. Chen, M. Zeng, J. Yunis, Y. Wei, Y. Wan, N. Wang, M. Zhou, C. Qiu, Q. Zeng, H.S. Ong, H. Wang, F.V. Makota, Y. Yang, Z. Yang, N. Wang, J. Deng, C. Shen, Y. Xia, L. Yuan, Z. Lian, Y. Deng, C. Guo, A. Huang, P. Zhou, H. Shi, W. Zhang, H. Yi, D. Li, M. Xia, J. Fu, N. Wu, J.B. de Haan, N. Shen, W. Zhang, Z. Liu, D. Yu, Selenium-GPX4 axis protects follicular helper T cells from ferroptosis, Nat. Immunol. 22 (9) (2021) 1127–1139, https://doi.org/10.1038/s41590-021-00996-0.

[42] F. Ren, X. Guo, R. Zhang, S. Wang, H. Zuo, Z. Zhang, D. Geng, Y. Yu, M. Su, Effects of selenium and iodine deficiency on bone, cartilage growth plate and chondrocyte differentiation in two generations of rats, Osteoarthr. Cartilage 15 (10) (2007) 1171–1177, https://doi.org/10.1016/j.joca.2007.03.013.

[45] S.J. Dixon, K.M. Lemberg, M.R. Lamprecht, R. Skouta, E.M. Zaitsev, C.E. Gleason, D.N. Patel, A.J. Bauer, A.M. Cantley, W. Yang, B.R. Morrison, B.R. Stockwell, Ferroptosis: an iron-dependent form of nonapoptotic cell death, Cell 149 (5) (2012) 1060–1072, https://doi.org/10.1016/j.cell.2012.03.042.

[46] S. Ding, X. Chu, Y. Jin, J. Jiang, X. Zhao, M. Yu, Epigallocatechin gallate alleviates high-fat diet-induced hepatic lipotoxicity by targeting mitochondrial ROS-mediated ferroptosis, Front. Pharmacol. 14 (2023), 1148814, https://doi.org/10.3389/fphar.2023.1148814.

[47] X. Yao, K. Sun, S. Yu, J. Luo, J. Guo, J. Lin, G. Wang, Z. Guo, Y. Ye, F. Guo, Chondrocyte ferroptosis contribute to the progression of osteoarthritis, J. Orthop. Translat. 27 (2021) 33–43, https://doi.org/10.1016/j.jot.2020.09.006.

[48] X. Zhou, Y. Zheng, W. Sun, Z. Zhang, J. Liu, W. Yang, W. Yuan, Y. Yi, J. Wang, J. Liu, D-mannose alleviates osteoarthritis progression by inhibiting chondrocyte ferroptosis in a HIF-2α-dependent manner, Cell Prolif. 54 (11) (2021), e13134, https://doi.org/10.1111/cpr.13134.

[49] H. Song, K.H. Park, Regulation and function of SOX9 during cartilage development and regeneration, Semin. Cancer Biol. 67 (Pt 1) (2020) 12–23, https://doi.org/10.1016/j.semcancer.2020.04.008.